Hindawi
Advances in Materials Science and Engineering
Volume 2021, Article ID 8582274, 8 pages
https://doi.org/10.1155/2021/8582274

Research Article

Phase, Microstructure, Thermochromic, and Thermophysical Analyses of Hydrothermally Synthesized W-Doped VO_2 Nanopowder

Hamdi Muhyuddin Barra[1], **Soo Kien Chen**[2], **Nizam Tamchek**[2], **Zainal Abidin Talib**[2], **Oon Jew Lee**[3], and **Kar Ban Tan**[4]

[1]*Department of Physics, College of Natural Sciences and Mathematics, Mindanao State University, Marawi City 9700, Philippines*
[2]*Department of Physics, Faculty of Science, Universiti Putra Malaysia, 43400 UPM Serdang, Selangor, Malaysia*
[3]*Advanced Nano Materials (ANoMa) Research Group, Faculty of Science and Marine Environment, Universiti Malaysia Terengganu, 21300 Kuala Nerus, Terengganu, Malaysia*
[4]*Department of Chemistry, Faculty of Science, Universiti Putra Malaysia, 43400 UPM Serdang, Selangor, Malaysia*

Correspondence should be addressed to Hamdi Muhyuddin Barra; hmdbarra@msumain.edu.ph

Received 4 June 2021; Accepted 28 August 2021; Published 13 September 2021

Academic Editor: Lingxue Kong

Vanadium dioxide (VO_2) has great potential as an intelligent architectural glazing system as it can control the amount of light, heat, and solar energy relative to the temperature in the environment. However, the applicability of VO_2 for commercial use is yet to be realized because its phase transition temperature (τ_c) of ~68°C is too high for use in buildings. A proven strategy to lower its τ_c is by elemental doping. Hence, in this study, hydrothermal synthesis of nanostructured VO_2 was carried out with the introduction of tungsten (W) as a dopant. Furthermore, the effects of W doping on the structural, thermochromic, and thermophysical properties of VO_2 were examined. Using X-ray diffraction (XRD), it was found that the addition of W atoms affected the VO_2 lattice since the crystal structure of VO_2 was changed from monoclinic to tetragonal rutile. Subsequently, this influenced the thermochromic behavior of the prepared VO_2. Based on the differential scanning calorimetry (DSC), doping with tungsten resulted in a significant decrease in τ_c from 66.47°C to as low as 31.64°C. Moreover, W doping affected the thermophysical properties of the samples. Accordingly, an abrupt increase in the thermal conductivities of the doped samples was observed across the transition temperature.

1. Introduction

Energy-saving methods are important in curbing the problem of global climate change. One way to conserve energy is by enhancing energy efficiency, i.e., minimizing avoidable energy losses while maximizing its output [1]. Consequently, one of the areas where efficiency can be greatly improved is in built environments or buildings as they use up a significant amount of energy. In fact, buildings consume about 30–40% of the world's primary energy, mainly for heating, ventilation, and air conditioning (HVAC), lighting, and appliance usage [2]. However, the majority of this energy is wasted due to the inefficiencies of windows. Since windows easily allow heat to go in or out of a building, more energy is required to use cooling or heating systems to balance the increase or decrease in temperature [3].

A promising avenue in reducing energy expenditure and losses in buildings is the fabrication of energy-efficient windows with the ability to control the throughput of light, heat-carrying infrared (IR) radiation, and solar energy. One way to do this is by coating spectrally selective materials on the surface of windows [4]. By blocking unwanted and regulating solar radiation, usage of HVAC and lighting can be minimized, which can translate into reductions in energy use and greenhouse gas (GHG) emissions.

A prime candidate for this application is the thermochromic compound vanadium dioxide (VO_2), as it has the ability to reversibly change from a semiconductor with a monoclinic structure (M-phase) to a metal with a tetragonal rutile structure (R-phase) at a phase transition temperature (τ_c) of 68°C [5]. As the material undergoes a phase shift, its optical properties also change; i.e., when it is in the VO_2 (M) phase, it is transparent to IR radiation, whereas when it is in the VO_2 (R) phase, it becomes IR reflective [6]. Meanwhile, the transmission of visible light does not change in both phases [7]. Hence, VO_2 has great potential in the fabrication of smart windows.

However, the industrial and commercial use of VO_2 have yet to be realized due to some limiting factors [8]. For instance, the τ_c of VO_2 is still too high for near room temperature usage in buildings. Ideally, VO_2-based windows should reflect heat-carrying IR rays at room temperature (~25°C) to achieve people's thermal comfort [9]. Doping VO_2 has been reported to be the most effective way of lowering the τ_c value of VO_2 [10]. Cations such as niobium (Nb^{5+}), tantalum (Ta^{5+}), molybdenum (Mo^{6+}), and tungsten (W^{6+}), which have a larger radius than V^{4+} ion and high valency, are primary candidates for such task [11].

For instance, in the case of tungsten, Long et al. comprehensively discussed the effects of W dopant on the atomic structure of VO_2 and the reduction of τ_c by employing X-ray absorption spectroscopy using synchrotron radiation coupled with first-principle calculations [12]. Accordingly, there is intrinsic symmetry around the local structure of the W atom with a seemingly tetragonal configuration. This propels the distortion and twisting of the asymmetric VO_2 lattice forming rutile-like nuclei that cause a reduction in the thermal activation energy of the phase transition. This is evident in the works of Chen et al. (2012) and Blackman et al. when both groups doped VO_2 with W and reported a reduced τ_c of 35°C and 20°C, respectively [13, 14]. Most recently, W doping was done by Zou et al. (2018) by a combined sol-gel-hydrothermal-annealing process that further reduced τ_c to 27°C with a temperature reduction rate of -22 C$\underline{o}$/at% W [15]. Meanwhile, Hanlon et al. used molybdenum as VO_2 dopant and found that the phase transition temperature of VO_2 decreases to 24°C with a rate of 5 C$\underline{o}$/at% Mo [16]. Moreover, codoping of W and Mo was conducted by Lv et al. (2014), using microwave-assisted HT synthesis, which led to further reduction of τ_c to as low as 17°C [17].

Overall, these studies have mostly reported on the reduction of the transition temperature of VO_2 to near room temperature by elemental doping. However, very few studies have analyzed the effects of doping on the phase transition performance of VO_2. Additionally, there is a notable paucity of studies assessing the effects of doping on the thermophysical properties of VO_2, particularly across its phase transition temperature. Hence, in this work, the effects of tungsten as dopant on the structural and thermochromic properties of VO_2 were examined. In particular, the phase transition performance of doped VO_2 was evaluated by measuring its enthalpy and hysteresis. Further, the effects of the dopant on the thermophysical properties of the prepared nanostructured VO_2 were investigated.

2. Materials and Methods

2.1. Sample Preparation. All chemical reagents in this study were of analytical grade and used without further purification. Differing weight percentages (wt%) of metallic tungsten powder relative to the V precursor were prepared. This was done by dissolving the requisite amount of W in 2 mL hydrogen peroxide (H_2O_2, 30%). The concentration of the dopant relative to the V precursor, wt% (W), was calculated using the following equation:

$$\text{wt\%}\,(W) = \frac{m(W)}{m(W) + m(V)} x100\%, \qquad (1)$$

where m(W) is the mass of the dopant and m(V) is the mass of the V precursor. W concentrations of 1, 1.5, 2, and 3 wt% were prepared for the hydrothermal process, and the respective powder products were labeled as VMW1%, VMW1.5%, VMW2%, and VMW3%. Also, the undoped sample was labeled VMW0% to denote the absence of dopant.

The preparation of the undoped sample is reported elsewhere [18]. Meanwhile, to begin the synthesis of the doped samples, 2.4750 g of V_2O_5 was dissolved in 148 mL deionized water under magnetic stirring. $H_2C_2O_4$ with a mass of 4.9502 was then added while vigorous stirring continued. When the V_2O_5-$H_2C_2O_4$-H_2O system turned blue-green, the W-H_2O_2 solution was added to it. Afterwards, the solution was transferred into a 240 mL Teflon-lined autoclave when it changed into a reddish color. It was then heated inside an electric oven at a temperature and processing time of 180°C and 24 h, respectively. Then, the blue-black precipitate was collected after cooling it to ambient temperature. Then, it was centrifuged and washed with ethanol and water several times. Finally, the powder was dried at 60°C overnight. Since the produced VO_2 particles were in a metastable state, further heat treatment was employed to obtain the desired thermodynamically stable phase. Hence, the samples were calcined at 650°C in 2 hours under an N_2 environment with heating and cooling rates of 5 C°/min.

2.2. Sample Characterization. The phase and crystal structure of the prepared samples were analyzed by X-ray diffraction using the X'pert Pro PANalytical MPD diffractometer at 2θ values ranging between 20° and 80° at a scanning step rate of 0.017 s^{-1}. Additionally, the morphology of the samples was examined by field-emission scanning electron microscopy (FESEM) using a JEOL-JSM7600F scanning electron microscope at an acceleration voltage of 5 kV. Meanwhile, differential scanning calorimetry (DSC) was employed to measure the obtained powder's thermochromic properties. This was done by placing an amount of nanopowder in a DSC822e (Mettler Toledo) specimen pan with a temperature accuracy of ±0.20°C. As the temperature was increased from 30°C to 200°C and then decreased from 200°C to 30°C, the heat flow on the sample was measured. Finally, thermal diffusivity was measured using a Netzsch LFA457 light flash apparatus (LFA). This was done by molding the nanopowder samples into pellets with a thickness of 1 mm and a diameter of 10 mm using a hydraulic press.

3. Results and Discussion

3.1. Phase and Structural Analysis. The XRD scans of the hydrothermally prepared undoped and W-doped VO_2 powders after annealing are illustrated in Figure 1. The appearance of a non-VO_2 compound was observed from sample VMW1%, as shown in the presence of V_6O_{13}. These crests gradually diminish as the concentration of the dopant was increased. However, peaks belonging to $V_{2.4}W_{0.6}O_7$ began to appear at wt. percentage of 1.5 wt%. Interestingly, when the concentration of W reached 2 wt%, peaks associated with the tetragonal rutile VO_2 (*R*) were detected with ICSD code 98-007-1662 of space group P42/mnm. As found in literature, replacing a V site in the VO_2 crystalline structure with the larger W atom causes strong interactions. Subsequently, the asymmetric atoms in the VO_2 lattice rearrange themselves, which leads to the transformation from monoclinic to tetragonal configuration.

Moreover, an enlarged view of the preceding XRD patterns is illustrated in Figure 2 to provide a magnified look at the effects of the doping concentration on the phase formations in VO_2 (*M*). At 2θ values between 26° and 35°, as many as four *events* or changes (labeled *I*, *II*, *III*, and *IV*) in the XRD plots can be observed. Firstly, in *event I*, the (0 1 1) peak of VO_2 (*M*) at 26.90° deteriorated, and a new peak at 27.11°, which belongs to $V_{2.4}W_{0.6}O_7$, appeared. In *event II*, the VO_2 (*M*) peak at 27.86° shifted position gradually to 27.65°, which can be indexed to the VO_2 (*R*) peak with Miller indices (hkl) of (1 1 0). Also, the appearance and abrupt disappearance of the peak associated with V_6O_{13} can be seen in *event III*. The presence of V_6O_{13}, which signified the occurrence of oxidation in an otherwise inert nitrogen atmosphere, may have stemmed from the residual H_2O_2 molecules, which were not fully dissolved during the hydrothermal synthesis nor removed through the washing and centrifugation processes. Potentially, these molecules were adsorbed in the VO_2 (B) molecules and tended to reoxidize the VO_2 particles into V_6O_{13} during the heating treatment. Finally, in *event IV*, a VO_2 (*M*) peak gradually diminished while a new peak belonging to VO_2 (*R*) emerged. This shifting of peak to lower 2θ value is mainly due to the replacement of W atoms on the V sites. Considering that tungsten has a greater atomic radius (1.37 Å) compared with vanadium atom (1.34 Å), this can potentially result in the increase of adjacent interplanar distance (d-spacing). Hence, the peak position movement is towards the left because there is an inverse proportionality relationship between the d-spacing and 2θ values based on Bragg's law.

Additionally, the samples' full width at half maximum (FWHM) and lattice properties at the peak with the greatest intensity were measured and summarized in Table 1. It can be observed that the quality of crystallization diminished as the W content was increased to 2 and 3 wt.%. Specifically, the FWHM widened from 0.1299° to 0.1948° with increasing W concentration. A factor that affected the FWHM was the crystallite size which significantly decreased from 81.5 nm (for the undoped sample) to 50.1 nm (for sample VMW3%).

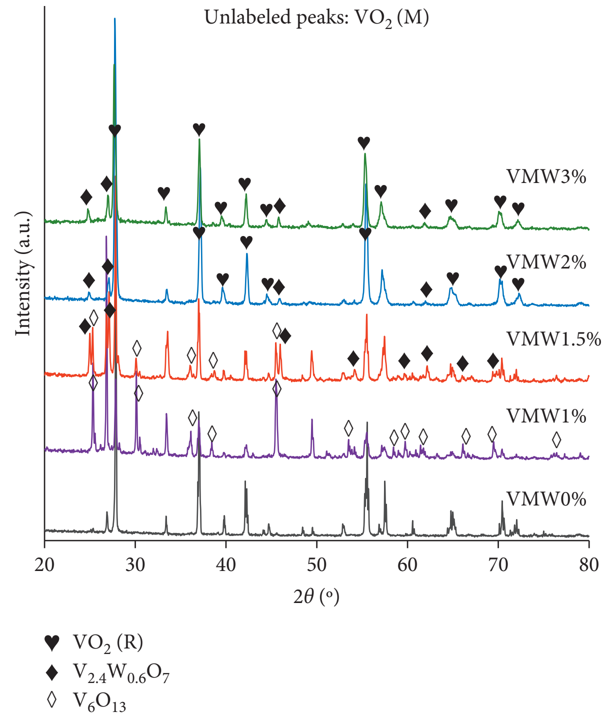

Figure 1: XRD scans of the undoped and W-doped samples.

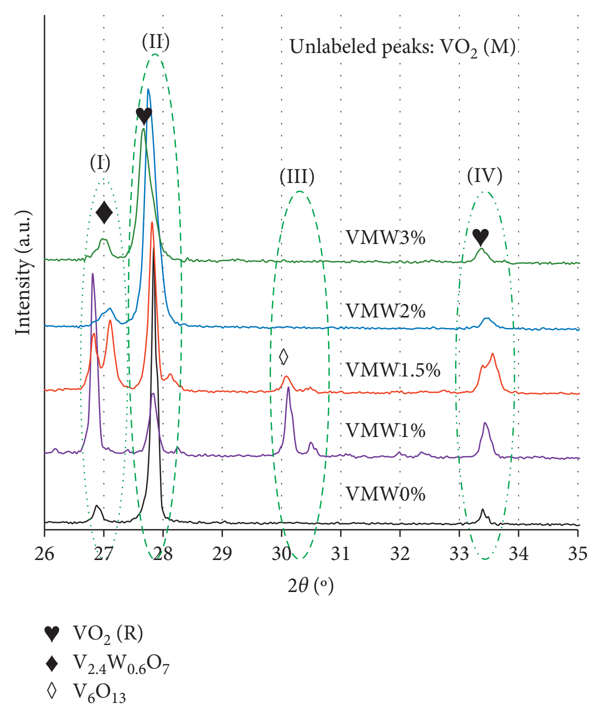

Figure 2: XRD scans at 2θ range between 26° and 35° for the undoped and W-doped VO_2 samples.

Table 1: FWHM and lattice properties of the undoped and W-doped VO_2 samples.

Sample	W conc. (wt.%)	FWHM (o)	Crystallite size, (nm)	Lattice strain LS (%)	d-Spacing (Å)
VMW0%	0	0.130	81.5	0.196	3.203
VMW1%	1	0.130	81.5	0.216	3.205
VMW1.5%	1.5	0.130	81.5	0.197	3.206
VMW2%	2	0.195	50.1	0.321	3.214
VMW3%	3	0.195	50.1	0.322	3.225

Based on the transformation of VO_2 (B) to VO_2 (R) during the annealing process, the increase in temperature resulted in the breakage of the interconnections between the edge-sharing and corner-sharing octahedra in the VO_2 (B) crystal lattice. Then, the octahedra underwent reorientation to form the rutile tetragonal structure, which has a smaller crystallite size. Moreover, the addition of tungsten accelerated this process. As elucidated in the work of Zhang et al. (2015), distortions caused by the tungsten atoms in the doped VO_2 (B) hasten the breakage of the interconnecting V-O octahedra [19]. With prolonged heating during the annealing stage, the VO_2 (B) transformed to VO_2 (R) at a faster rate, which resulted in the growth of VO_2 (R) with reduced crystallite size.

Another factor that caused the broadening of peaks was the internal strain in the VO_2 lattice which increased from 0.196 to 0.322. This increase is mainly due to the difference in the atomic radius of W and V. By replacing V sites with W atoms, which have a greater radius, distortions in the V-V and V-O bonds in the VO_2 (M) crystals transpire. With increasing dopant concentration, more V sites were replaced with W atoms, thus resulting in greater lattice strain. This finding is further supported by the measurement of the interplanar spacing in the undoped and W-doped samples. As shown in the rightmost column of Table 1, the d-spacing increased with increasing W weight percentage. Indeed, this shows the successful partial substitution of V atoms with W atoms in the VO_2 (M) crystal structure.

Additionally, the morphologies of the synthesized W-doped VO_2 were examined using field-emission scanning electron microscopy analysis. The FESEM scans of the samples are given in Figure 3. Similar to sample VMW0%, all the doped samples showed the formation of spherical shapes, albeit at larger sizes. Grain growth mechanism may have caused these changes in the morphology during the heat treatment process. Correspondingly, dissociation of the vanadium and oxygen atoms causes the disordering and breakage of the VO_2 (B) nanobelts. Then, the crystalline structure is reconfigured and transformed into the monoclinic VO_2 (M) or into the tetragonal VO_2 (R) with the addition of tungsten. After 2 hours of annealing, coalescing of the nanoparticles occurs. Agglomeration stage follows, whereby oblate, spherical, and/or plate-like shaped particles are formed. For samples VMW0%, VMW1%, VMW1.5%, VMW2%, and VMW3%, the measured average diameters of these spheroids were 0.24, 3.08, 2.17, 1.51, and 0.89 μm, respectively. According to Chen et al. (2014), this increase in grain size is a prominent feature of W doping on VO_2 [20]. Seemingly, samples with wt.% of 1% and 1.5% had rough surfaces compared with the undoped and the other doped samples. This may be due to the presence of V_6O_{13} based on their XRD scans. Meanwhile, the formation of nanorods can be noticed in Figures 3(c) and 3(d) when the doping reached 2 and 3 wt%. The widths of these rods were as low as 161 nm for VMW2% and 101 nm for VMW3%. Based on the diffractograms of these samples, these rods may contain the compound $V_{2.4}W_{0.6}O_7$.

3.2. Influence on Thermochromic Properties. The thermochromic behavior of W-doped VO_2 can be evaluated using the DSC curve of the samples in Figure 4. As seen, a change in the position of the peaks can be readily observed as the concentration of W was increased. Particularly, the peaks shifted to the left, indicating the reduction of the phase transition temperature. As elaborately discussed by Tan et al. (2012), the local structure of the tungsten atom has intrinsic symmetry with a tetragonal-like configuration [21]. When added to a VO_2 (M), W propels the distortion of the VO_2 lattice and twisting of the asymmetric V-V bonds, resulting in the formation of rutile-like nuclei. Consequently, this lowers the thermal activation energy, thereby causing the reduction of the phase transition. Also, sample VMW3% exhibited two sharp peaks at 31.64°C and 51.99°C. These lower phase transition temperatures may be caused by the increase in VO_2 (R) contained in the sample compound as evidenced in the sample's XRD scan in Figure 1. Also, as reported by Xu et al. (2020), the presence of different-shaped VO_2 nanoparticles can lead to multiple phase transition peaks [22]. Indeed, nanoparticles with differing shapes and sizes can be observed in sample VMW3% in Figure 3(e). However, in the cooling direction, only a single peak was observed. This can be explained through the work of Zou et al. (2018). Accordingly, heating a W-doped VO_2 (M) nanoparticles causes recrystallization which may transform the nanoparticles into larger-sized VO_2 [15]. By heating the sample to 200°C during the heat flow measurement in the DSC, larger-sized VO_2 may have formed. Subsequently, this resulted in higher phase transition temperature in the cooling direction with a single peak.

Furthermore, the measured values of the phase transition temperatures of the samples based on the DSC curve are recorded in Table 2. Correspondingly, τ_c significantly decreased from 66.47°C to 47.35°C when the W concentration was increased to 3%. The decrease in the phase transition temperature can be attributed to the increase in lattice strain (Table 1) as well as the growth of VO_2 (R), as evidenced by the XRD scan (Figure 1). Meanwhile, to determine the heat of metal-to-semiconductor transition and strength of phase change, the enthalpies and hysteresis of the samples were

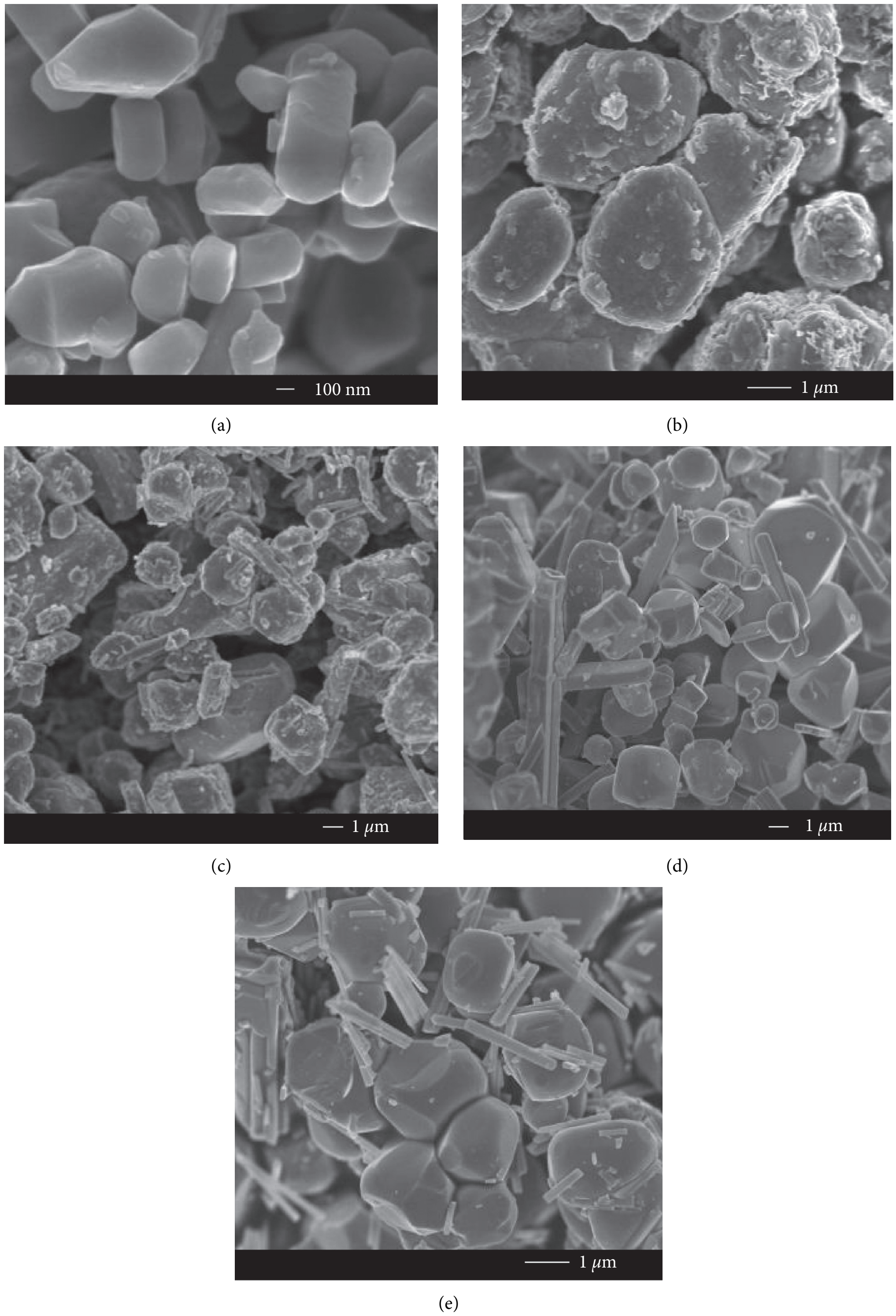

Figure 3: FESEM scans of W-doped VO_2 at differing dopant weight percentages of (a) 0, (b) 1, (c) 1.5, (d) 2, and (e) 3 wt%.

measured (see Table 2). As seen, a large increase in hysteresis is observed as the doping wt.% increases. Since hysteresis is mainly affected by crystallinity and grain size, the high hysteresis in the doped samples may have resulted from the low quality of crystallization due to the presence of impurities in the forms of V_6O_{13} and $V_{2.4}W_{0.6}O_7$ (see Figure 2) as well as their large grain size (refer to Figure 3).

Meanwhile, a decrease in enthalpy can be observed when 1 wt% W was added to the VO_2 sample. Then, an increasing trend occurred when the wt% of the dopant was increased to 2%. Finally, the heat of metal-semiconductor phase transition (MST) decreased when the W was at 3 wt.%. The trends in τ_c and ΔH of the samples are summarized in Figure 5. As seen, both the phase transition temperatures

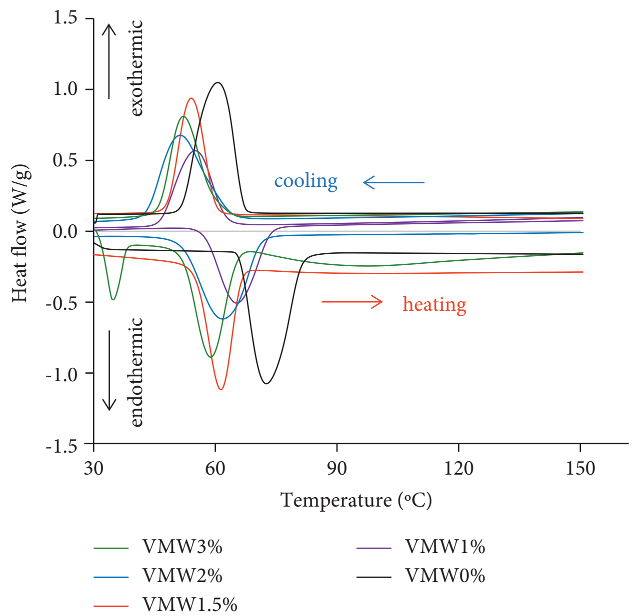

FIGURE 4: DSC curves of undoped and W-doped samples.

TABLE 2: Thermochromic properties of undoped and W-doped samples.

Sample	W conc. (wt%)	Phase transition (°C)			h (C°)	Enthalpy (J/g)		
		τ_{heat}	τ_{cool}	τ_c		ΔH_{heat}	ΔH_{cool}	ΔH
VMW0%	0	66.01	66.93	66.47	0.92	−53.77	54.22	54.00
VMW1%	1	57.24	62.05	59.65	4.81	−33.68	32.48	33.08
VMW1.5%	1.5	54.46	59.47	56.97	5.01	−35.24	36.46	35.85
VMW2%	2	51.62	61.71	56.67	10.09	−44.96	44.75	44.86
VMW3%	3	31.64; 51.99	58.41	47.35	6.42	−10.52;−37.47	38.67	28.89

$\tau_c = (\tau_{heat} + \tau_{cool})/2$, $h = |\tau_{heat} - \tau_{cool}|$, and $\Delta H = (|\Delta H_{heat}| + \Delta H_{cool})/2$.

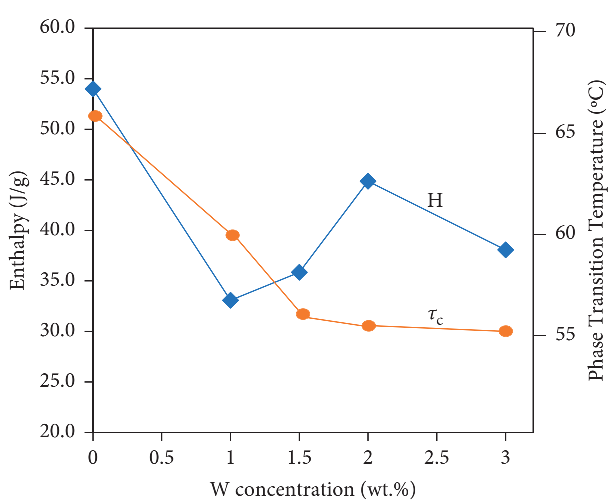

FIGURE 5: Phase transition temperature and enthalpy of VO_2 with varying W concentration.

and enthalpies of all doped samples were lower compared to the undoped sample. This is primarily due to the decrease in the thermal activation energy when W was introduced in the VO_2 (*M*) lattice. Based on the work of Liang et al. (2016), the V-V bonds in VO_2 (*M*) are arranged with interval distances of 2.65 and 3.12 Å, while in VO_2 (R), the V-V intervals are equidistant at 2.87 Å [23]. Accordingly, partial substitution of V atoms with W atoms, whose radius is greater, results in the shrinking of the V-V bond intervals. Thus, a decrease in the structural difference between the *M*- and *R*-phases of VO_2 emerges. Consequently, the activation energy of the metal-to-semiconductor transition decreases; hence, τ_c and ΔH of the doped sample are lower compared with the undoped VO_2 (*M*). Nonetheless, the values of the enthalpies in this work are closer to the values for bulk VO_2 (37.38 J/g – 51.85 J/g) [24]. Moreover, the decreasing trend in τ_c is mainly due to the increase in lattice strain, as shown in Table 1. Meanwhile, an increase in the enthalpy from 1 to 2 wt.% may be due to the removal of impurity in the form of V_6O_{13}, as displayed in the XRD pattern in Figure 2. Meanwhile, the decrease in enthalpy when the W concentration was changed from 2 to 3 wt.% can be potentially caused by the grain size effect considering that sample VMW3% has a greater grain size than VMW2%. Reasonably, the large grain size of VMW3% may contain structural defects or more oxygen vacancies, which have been reported to cause a decrease in the phase transition temperature and the rate of phase transition [25].

3.3. Influence on Thermophysical Properties. The effects of introducing a tungsten dopant on the thermophysical properties of VO_2 were carried out using the microflash method. Specifically, the thermal diffusivity (α) of the samples at temperatures of 25, 50, 100, and 150°C was measured, and the results are plotted in Figure 6. Accordingly, the changes in α from 25 to 50°C, 50 to 100°C, and 100 to 150°C were 0.091, 0.210, and 0.027 mm^2/s. Hence, it can be inferred that the heat transferring ability of the highly pure VO_2 (M) significantly increased across the phase transition temperature. Apart from sample VMW1%, an increase in α was still discernible across the metal-to-semiconductor transition temperature of the doped samples. Specifically, the measured $\Delta\alpha$ from 50 to 100°C were 0.113, 0.157, and 0.07 for samples with W concentrations of 1.5, 2, and 3 wt%. Meanwhile, doping generally resulted in a decrease in thermal diffusivity at a temperature above 25°C. As shown in Table 1, the d-spacing of the doped samples increased, which could result in the decrease of the transfer of heat in the VO_2 lattice.

Moreover, the thermal conductivity (κ) of the samples was calculated using the following equation:

$$\kappa = \rho\alpha C_p, \tag{2}$$

where ρ is the material's density and C_p is the heat capacity. The measured densities of the pelletized samples, namely, VMW0%, VMW1%, VMW1.5%, VMW2%, and VMW3%, were 2.75, 3.20, 3.23, 3.23, and 3.31 g/cm^3, respectively. Inasmuch as these pellets were obtained by the hydraulic pressing of porous nanopowder samples, their densities were lower than the theoretical density of VO_2 (M), which is 4.67 g/cm^3. The heat capacities, on the other hand, were determined from the DSC data in Figure 4, using the following equation:

$$C_p = \frac{Q/m}{dT/dt}, \tag{3}$$

where Q/m is the measured heat flow in the DSC curve and dT/dt is the temperature gradient employed in the DSC scan. The resulting measurements of κ are plotted in Figure 7.

Correspondingly, the profiles of these plots are similar to the results of Oh et al., albeit with lower values, which is primarily due to the low densities used in calculations [26]. Accordingly, a considerable increase in thermal conductivity across τ_c can be observed. Particularly, for the undoped VO_2, κ increased from 2.140 to 3.163 W/m•K as the temperature was increased from 50 to 100°C. This corresponded to a $\Delta\kappa$ of 1.023 W/m•K, which is greater than $\Delta\kappa$ from previous results on VO_2 bulk and nanobeams [27]. Meanwhile, for W-doped samples, the thermal conductivities at 25°C were very close to that reported by Oh et al. for VO_2 bulk. Also, an incremental change in κ occurred from 25 to 50°C. Then, a bigger jump can be observed across the phase transition temperature. Specifically, $\Delta\kappa$ with values of 0.297, 1.424, 1.329, and 1.288 W/m•K were recorded. In general, these values are greater compared to previous findings [13, 27]. This increase in thermal conductivity is possibly caused by the absence of grain boundary defects, which tend to decrease the thermal conductivity of a material.

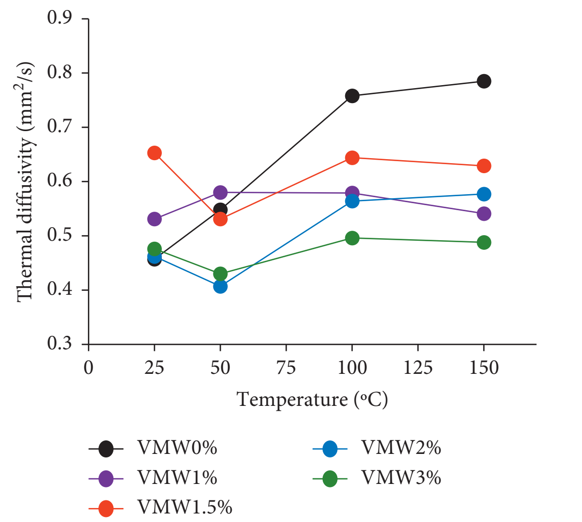

Figure 6: Thermal diffusivity of VO_2 at varying W concentration.

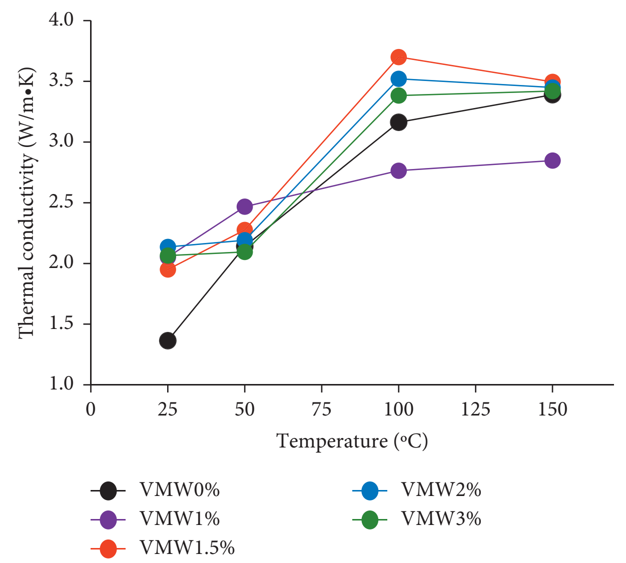

Figure 7: Thermal conductivity of undoped and W-doped VO_2.

4. Conclusions

Investigation of the influences of elemental doping on the structural, morphological, thermochromic, and thermophysical properties of VO_2 nanoparticles was carried out. Accordingly, the introduction of W shifted some of the peak locations in the XRD scans of the samples, which indicated a phase transformation from VO_2 (M) to VO_2 (R). This shift in phase was caused by the increase in the lattice strain of the VO_2 crystal structure. Also, an increase in grain size was observed in the doped sample. More importantly, doping resulted in the decrease of the phase transition temperature of VO_2 from 66.47°C to as low as 31.64°C. However, a decrease in the enthalpy was observed, which signified a decrease in the transition strength. This was potentially caused by many factors such as lower crystallinity, an increase in lattice strain, and the presence of impurities. In addition, W doping was found to influence the thermophysical properties of VO_2. In particular, the thermal diffusivity and thermal conductivity of the doped VO_2 increased noticeably across its phase transition temperature.

Data Availability

The data used to support the findings of this study are available from the corresponding author upon request.

Conflicts of Interest

The authors declare that they have no conflicts of interest.

Acknowledgments

The authors would like to thank the Universiti Putra Malaysia for the financial support of this research under Putra Grant GP-IPS (Grant no. 9501500).

References

[1] B. Baatz, G. Relf, and S. Nowak, "The role of energy efficiency in a distributed energy future," *The Electricity Journal*, vol. 31, no. 10, pp. 13–16, 2018.

[2] C. G. Granqvist, P. C. Lansåker, N. R. Mlyuka, G. A. Niklasson, and E. Avendaño, "Progress in chromogenics: new results for electrochromic and thermochromic materials and devices," *Solar Energy Materials and Solar Cells*, vol. 93, no. 12, pp. 2032–2039, 2009.

[3] M. Kamalisarvestani, S. Mekhilef, and R. Saidur, "Analyzing the optical performance of intelligent thin films applied to architectural glazing and solar collectors," in *Sustainability in Energy and Buildings*, A. Hakansson, M. Hojer, R. Howlett, and L. Jain, Eds., Springer, Berlin, Germany, pp. 813–826, 2013.

[4] Y. Gao, H. Luo, Z. Zhang et al., "Nanoceramic VO_2 thermochromic smart glass: a review on progress in solution processing," *Nano Energy*, vol. 1, no. 2, pp. 221–246, 2012.

[5] M. M. Seyfouri and R. Binions, "Sol-gel approaches to thermochromic vanadium dioxide coating for smart glazing application," *Solar Energy Materials and Solar Cells*, vol. 159, pp. 52–65, 2017.

[6] J. Wu, W. Huang, Q. Shi et al., "Effect of annealing temperature on thermochromic properties of vanadium dioxide thin films deposited by organic sol-gel method," *Applied Surface Science*, vol. 268, pp. 556–560, 2013.

[7] L. Long and H. Ye, "How to be smart and energy efficient: a general discussion on thermochromic windows," *Scientific Reports*, vol. 4, pp. 1–10, 2014.

[8] S. Li, G. A. Niklasson, and C. G. Granqvist, "Nanothermochromics: calculations for VO_2 nanoparticles in dielectric hosts show much improved luminous transmittance and solar energy transmittance modulation," *Journal of Applied Physics*, vol. 108, Article ID 063525, 2010.

[9] M. Kamalisarvestani, R. Saidur, S. Mekhilef, and F. S. Javadi, "Performance, materials and coating technologies of thermochromic thin films on smart windows," *Renewable and Sustainable Energy Reviews*, vol. 26, pp. 353–364, 2013.

[10] P. Kiri, G. Hyett, and R. Binions, "Solid state thermochromic materials," *Advanced Materials Letters*, vol. 1, no. 2, pp. 86–105, 2010.

[11] S. Wang, M. Liu, L. Kong, Y. Long, X. Jiang, and A. Yu, "Recent progress in VO_2 smart coatings: strategies to improve the thermochromic properties," *Progress in Materials Science*, vol. 81, pp. 1–54, 2016.

[12] R. Long, B. Qu, R. Tan et al., "Identifying structural distortion in doped VO_2 with IR spectroscopy," *Physical Chemistry Chemical Physics*, vol. 14, no. 20, pp. 7225–7228, 2012.

[13] J. Chen, X. Liu, X. Yuan et al., "Investigation of the thermal conductivities across metal-insulator transition in polycrystalline VO_2," *Chinese Science Bulletin*, vol. 57, no. 26, pp. 3393–3396, 2012.

[14] C. S. Blackman, C. Piccirillo, R. Binions, and I. P. Parkin, "Atmospheric pressure chemical vapour deposition of thermochromic tungsten doped vanadium dioxide thin films for use in architectural glazing," *Thin Solid Films*, vol. 517, no. 16, pp. 4565–4570, 2009.

[15] J. Zou, X. Chen, and L. Xiao, "Phase transition performance recovery of W- doped VO_2 by annealing treatment," *Materials Research Express*, vol. 5, Article ID 065055, 2018.

[16] T. J. Hanlon, J. A. Coath, and M. A. Richardson, "Molybdenum-doped vanadium dioxide coatings on glass produced by the aqueous sol-gel method," *Thin Solid Films*, vol. 436, no. 2, pp. 269–272, 2003.

[17] W. Lv, D. Huang, Y. Chen, Q. Qiu, and Z. Luo, "Synthesis and characterization of Mo-W co-doped VO2(R) nano-powders by the microwave-assisted hydrothermal method," *Ceramics International*, vol. 40, no. 8, pp. 12661–12668, 2014.

[18] H. M. Barra, S. K. Chen, N. Tamchek, Z. A. Talib, O. J. Lee, and K. B. Tan, "Nanostructured VO_2 (A) and VO_2 (M) derived from VO_2 (B): facile preparations and analyses of structural, thermal, optical and thermophysical properties," *Materials Science*, vol. 27, no. 3, pp. 269–275, 2021.

[19] Y. Zhang, X. Tan, C. Huang, and C. Meng, "Hydrothermal treatment with VO_2(B) nanobelts for synthesis of VO_2(A) and W doped VO_2(M) nanobelts," *Materials Research Innovations*, vol. 19, no. 4, pp. 295–302, 2015.

[20] Z. Chen, Y. Gao, L. Kang, C. Cao, S. Chen, and H. Luo, "Fine crystalline VO_2 nanoparticles: synthesis, abnormal phase transition temperatures and excellent optical properties of a derived VO_2 nanocomposite foil," *Journal of Materials Chemistry*, vol. 2, no. 8, pp. 2718–2727, 2014.

[21] X. Tan, T. Yao, R. Long et al., "Unraveling metal-insulator transition," *Science. Reports. UK*, vol. 2, pp. 1–6, 2012.

[22] C. Xu, G. Liu, M. Li et al., "Optical switching and nanothermochromic studies of VO_2 (M) nanoparticles prepared by mild thermolysis method," *Materials & Design*, vol. 187, Article ID 108396, 2020.

[23] S. Liang, Q. Shi, H. Zhu, B. Peng, and W. Huang, "One-step hydrothermal synthesis of W-doped VO_2 (M) nanorods with a tunable phase-transition temperature for infrared smart windows," *ACS Omega*, vol. 1, no. 6, pp. 1139–1148, 2016.

[24] Y. Chen, S. Zhang, F. Ke et al., "Pressure-temperature phase diagram of vanadium dioxide," *Nano Letters*, vol. 17, no. 4, pp. 2512–2516, 2017.

[25] J. Y. Suh, R. Lopez, L. C. Feldman, and R. F. Haglund, "Semiconductor to metal phase transition in the nucleation and growth of VO_2 nanoparticles and thin films," *Journal of Applied Physics*, vol. 96, no. 2, pp. 1209–1213, 2004.

[26] D. Oh, C. Ko, and S. Ramanathan, "Thermal conductivity and dynamic heat capacity across the metal-insulator transition in thin film VO_2," *Applied Physics Letters*, vol. 96, pp. 1–4, 2010.

[27] S. Lee, K. Hippalgaonkar, F. Yang et al., "Anomalously low electronic thermal conductivity in metallic vanadium dioxide," *Science*, vol. 355, no. 6323, pp. 371–374, 2017.